https://doi.org/10.37434/tpwj2022.04.08

APPLICATION OF FRACTAL ANALYSIS IN DIAGNOSTICS OF TECHNICAL CONDITION OF METAL STRUCTURE ELEMENTS

V.V. Usov[1], M.D. Rabkina[2], N.M. Shkatulyak[1], N.I. Rybak[1], O.O. Stofel[3]

[1]K.D. Ushinskyi South-Ukraine National Pedagogical University
26 Staroportofrankivska Str., 65020, Odessa, Ukraine
[2]E.O. Paton Electric Welding Institute of the NASU
11 Kazymyr Malevych Str., 03150, Kyiv, Ukraine
[3]National Technical University of Ukraine «Igor Sikorsky Kyiv Polytechnic Institute»
37 Peremohy Ave., 03056, Kyiv, Ukraine

ABSTRACT

It is shown that fractal analysis, as an additional tool of technical diagnostics and nondestructive testing, allows determination of the most important features of the condition and behaviour of metal structure elements during their operation and failure. Examples of application of fractal dimension of the fractures are presented, in order to assess the critical dimension of brittle cracks and to determine its effect on impact toughness, yield limit, ultimate strength, and failure pressure at hydraulic testing, and to detect the interrelation of fractal dimension with fatigue life after low-cycle fatigue fracture of metal of pipeline welded joints. It is found that the nature of fractal dimensions of the fractures and diagrams of time dependence of the applied load at impact loading is due to the direction of cutting and temperature of testing the specimens. It is shown that the main component of {001} <110> texture of low-alloyed steel promotes an increase of fractal dimension of the fractures and development of brittle fracture at impact testing.

KEYWORDS: impact testing, fractal dimension, brittle crack, destruction

INTRODUCTION

Reliability of long-term application of metal structures largely depends on the approaches to determination of their technical condition, primarily, by nondestructive testing techniques. However, premature failure of structures may be due to presence of invisible defects, which promote degradation of physico-mechanical properties of the materials proper. It requires conducting mechanical testing of the specimens, in particular, on the selected samples.

Fractal analysis of the structure of metal and parts of metal structures for prediction of their failure at this stage has the role of an additional method of service life diagnostic. For instance, safe operation of oil and gas pipeline systems can be ensured, primarily, by studying the causes of pipeline failure, based on laboratory studies of base metal (BM) and metal of the characteristic zones of the welded joints (WJ).

Steel fracture is associated with such characteristics of steels as crystallographic texture, macro- and microstructure, ferrite-pearlite banding, structural component fraction, etc. [1, 2]. Experimental studies of the influence of the above structural characteristics on the regularities of elasto-plastic deformation, low-cycle fatigue fracture with involvement of physical methods of investigation (X-ray and fractographic analyses) are relevant. Therefore, the use of fractal analysis which shedying fracture surfaces is urgent [3].

The name ‘fractal’ comes from Latin “Fractus”, which means “fractional”. “broken”. When measuring the coast line length, it turned out that its length L depends on selection of measurement scale ℓ by the following relationship (in logarithmic coordinates):

$$L \infty \ell^{1-D}, \quad (1)$$

where D is the fractal dimension (FD) [4], which does not coincide with topological dimension d, is the fractional quantity and exceeds topological dimension d_i ($D > d$). For instance, for British coast line $D \approx 1.3$, and for Norwegian one $D \approx 1.5$. D value is the larger, the more rugged is the coast line [4]. It turned out that the structure of grain boundaries in metal polycrystals has a strong effect on the mechanical properties [5]. It is known that brittleness of metallic materials is often accompanied by intergranular fracture [6]. Avoiding intergranular fracture requires strengthening the grain boundaries by increasing their waviness [7]. The fractal dimension is the characteristic of grain boundary waviness.

EXPERIMENTAL PROCEDURE

DETERMINATION OF FRACTAL DIMENSION

One of the direct methods of determination of FD of two-dimensional images (microphotographs) of the

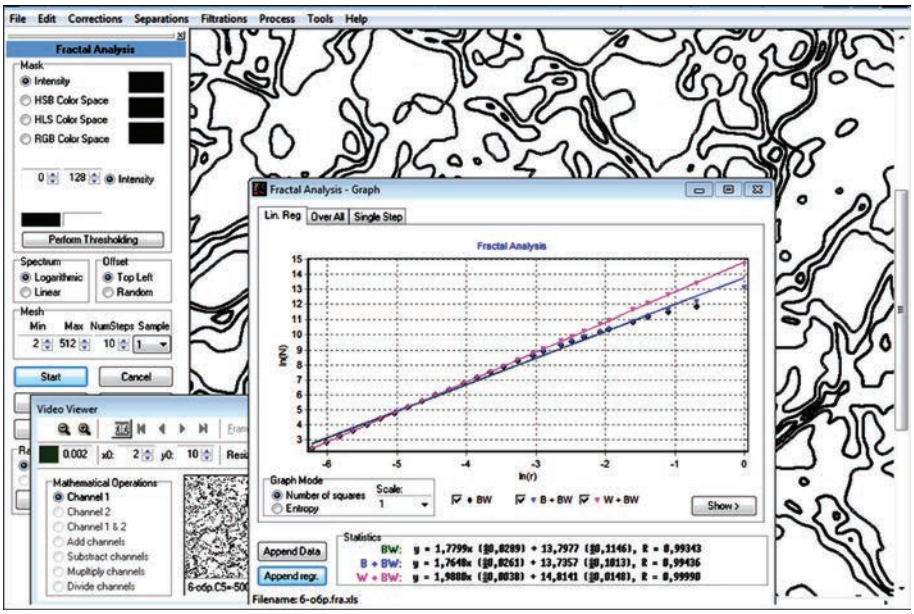

Figure 1. Example of determination of FD of a specimen of 20K grade steel after Charpy impact testing, using HarFa and ACDSee-PhotoStudioSoftware

fracture surface is the method of covering a plane curve with square grids, the dimensions of which are reduced a certain number of times (box-counting method) [8].

This method does not introduce distortions into the studied object. Here, fractal analysis of flat boundaries of fracture surface fragments is performed. A wide application of this method is due to the fact that it can be applied to any flat configuration [9]. For a mathematical fractal curve, FD coincides with Hausdorff dimension (HD). However, FD analytical calculation is rather labour-consuming and it is only possible in some cases. It is shown that fractal dimension, found using box-counting method in the case of dynamic systems, has the same values, as Hausdorff dimension [9].

In order to determine the fractal dimension, it is necessary to cover the image by elementary square grids with sides ℓ_i [9]. At each stage one and the same curve is covered by cells of a reduced scale. The smaller the square size, the more accurately is the curve reproduced. At the same time, the number of squares $N(\ell_i)$, crossed by the curve, is calculated. Then, the size of grid window ℓ_i is changed. The number of squares, crossed by the curve $N(\ell_2)$, $N(\ell_3)$ … $N(\ell_n)$. is calculated again. The number of squares $N(\ell_i)$, crossed by the curve, is related to the size of grid window ℓ_i by dependence [9]:

$$N(\ell) = \alpha^{\ell - D}, \qquad (2)$$

where $\lg N(\ell_i) = f(\lg \ell_i)$, $D = \lim\limits_{\ell \to 0} \dfrac{\lg N(\ell)}{\lg(1/\ell)}$ by definition is usually called fractal dimension or Hausdorff–Besicovich dimension [9]. Practically, D is determined by tangent of the angle of inclination of graphic dependence $\lg N(\ell_i) = f(\lg \ell_i)$ [9]. In order to determine the fractal dimension, it is convenient to apply HArFa software (Harmonic and Fractal Image Analysis), which is freely available [10]. Before determination of fractal dimension, fracture photos are usually cleared from the background, for instance, using ACDSee-PhotoStudioSoftware [11], in order to obtain only the lines of fracture fragment boundaries (Figure 1).

FRACTAL ANALYSIS OF BRITTLE FRACTURES

Fractal dimension of specimens from controlled rolled steel (Fe, 0.11 % C, 1.58 % Mn, 0.38 % Si) 20 mm thick after impact bend tests at temperatures from room to –110 °C was studied, and FD of wire from AD1 aluminium alloy after fatigue testing for symmetric bending was also determined at room temperature and at –10 °C.

Fracture surfaces were studied at the microlevel by microfractograms, obtained in scanning electron microscope REM-200 at 20000 magnification, and at the mezolevel — by optical microphotographs (MIM-7, 350 magnification).

On steel specimen fractures the fraction of the surface with brittle fracture was equal to 35 % at room temperature and 55 % at –70 °C. In aluminium fractures the "brittle" fraction increased up to 50 to 65 % at temperature lowering from 20 to –10 °C. Typical microphotograph of brittle fracture is shown in Figure 2. Fractal dimension of numbered section boundaries was determined.

It was found that the fractions after brittle fracture have average FD values of 1.20 ± 0.06 and 1.15 ± 0.06 for steel and aluminium, respectively. Proceeding from the assumption that in keeping with Griffit's cri-

terion at crack size increase by ΔR elastic energy is released, which is equal to increment of surface energy of the cut [13], the following dependence was derived for evaluation of critical dimensions of brittle cracks:

$$R^{2-D} \approx \frac{2\gamma DE}{\sigma^2}, \quad (3)$$

where E is the material modulus of elasticity, and $\gamma \approx 1$ is the specific surface energy [14].

Substitution into (3) of the data of studied steel testing at –70 °C (D_{av} = 1.2; E = 220 GPa [14], $\sigma \approx$ ≈ 100 MPa) yielded the value of critical size of fractal crack $R \approx 4.5$ μm, that corresponds to average size of cellular dislocation structure of steel [1] and agrees well with layered-brittle fracture by the mechanism of brittle transcrystalline cleavage (Figure 2).

A similar evaluation for brittle fracture of aluminium at $D_{av} \approx 1.15$, E = 70 GPa [15] and $\sigma \approx 20$ MPa (by impact toughness) yielded $R \approx 6.75$ μm.

FRACTAL DIMENSION OF GRAIN BOUNDARIES AND MECHANICAL PROPERTIES OF OXYGEN CYLINDER METAL

40 l oxygen cylinders from Dc steel (GOST 949–73) with different service life were studied at working pressure of 14.7 MPa.

Fractal dimension of grain boundaries of Dc steel of oxygen cylinders with different service life from 18 to 52 years varies from 1.10 to 1.14. Correlations of fractal dimension of grain boundaries with impact toughness, bursting pressure and yield limit with correlation coefficient R of not less than 0.80 were established (Figure 3).

Curves in Figure 3 correspond to regression equations with a high degree of correlation R:

$$KCV(-10\ ^\circ\text{C}) = (-1.14\cdot10^4 + 26.03\, D_{av}^{93.98})/(32.14 + D_{av}^{93.98}); \quad R = 0.92; \quad (4)$$

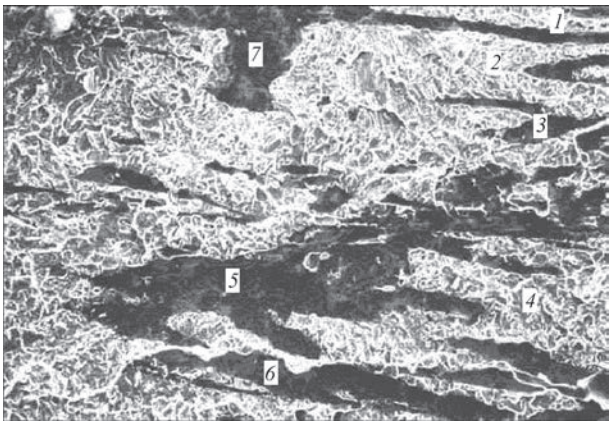

Figure 2. Electron microfractogram of layered-brittle fracture of steel after impact bend testing

$$KCV(20\ ^\circ\text{C}) = (-1.30\cdot10^5 + 38.29\, D_{av}^{164.73})/(820.64 + D_{av}^{164.73}); \quad R = 0.96; \quad (5)$$

$$P(20\ ^\circ\text{C}) = (5.34\cdot10^{-3} + 2.28\cdot10^4\, D_{av}^{184.77})/(1.10\cdot10^{-4} + D_{av}^{184.77}); \quad R = 0.80; \quad (6)$$

$$\sigma_{0.2} = (-1.53\cdot10^8 + 5.18\cdot10^2\, D_{av}^{152.92})/(8.09\cdot10^2 + D_{av}^{152.92}); \quad R = 0.80. \quad (7)$$

Correlation analysis of ultimate strength σ_t of cylinder metal indicates the absence of its connection with FD of the grain boundaries. The regression equation has the following form:

$$\sigma_t = 710.28; \quad R = 0.02. \quad (8)$$

FRACTAL FEATURES OF LOW-CYCLE FATIGUE FRACTURE (LCF) OF METAL OF PIPELINE WELDED JOINTS

Laboratory specimens for experimental determination of the main regularities of cyclic elasto-plastic deformation of base metal (BM) and metal of the characteristic welded joint zones, namely heat-affected zone (HAZ) and weld metal (WM), were cut out in the transverse direction from 530×8 mm pipe of the main pipeline from 17G1S-U steel after prolonged service

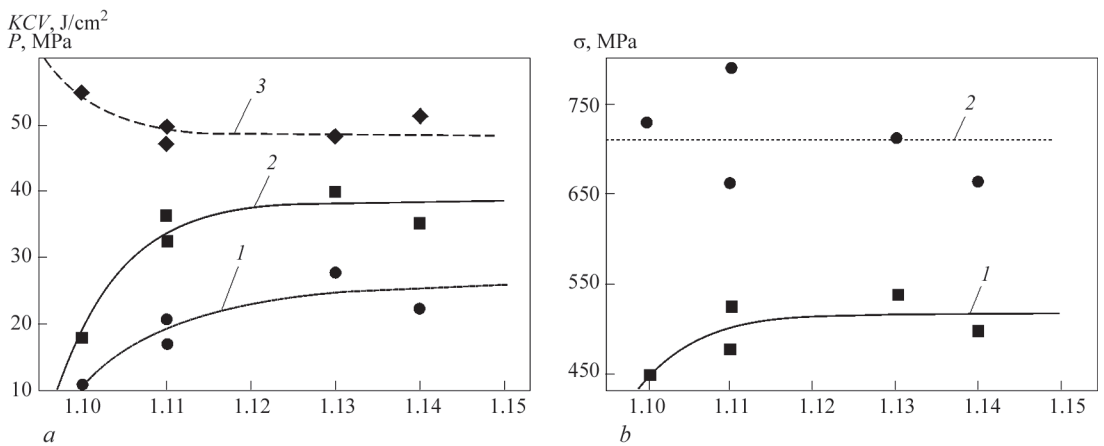

Figure 3. Correlation ties of average FD D_{av} of the grain boundaries: *a* — with *KCV* impact toughness at –10 °C (curve *1*) and 20 °C (curve *2*), bursting pressure (curve *3*); *b* — with yield limit $\sigma_{0.2}$ (curve *1*) and ultimate strength σ_t (curve *2*)

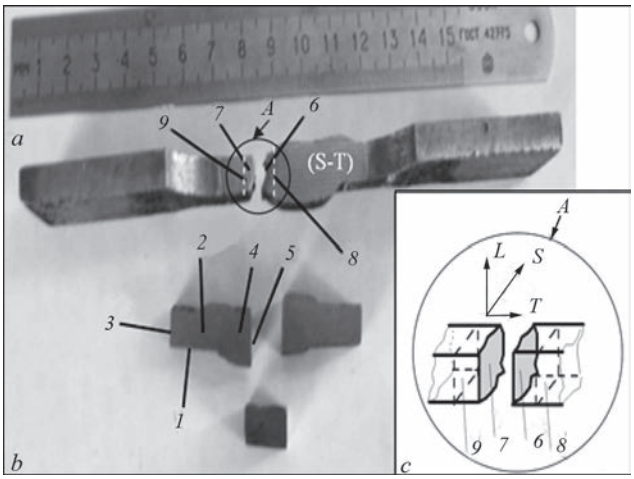

Figure 4. Studied texture sections: *a* — undeformed section (*1* — BM in *LT* rolling plane; *2*, *3* — BM in *ST* and *SL* planes; *4*, *5* — WM crossing in *ST* and *SL* planes); *b* — after fracture (*6*, *7* — bonded WM fracture surfaces; *8*, *9* — WM crossing in *SL* plane under the fractures); *c* — scheme of fragment *A* from Figure 3, *b*; *L* — longitudinal direction; *T* — transverse direction; *S* — direction, normal to *L* and *T* directions

[17]. Figure 4 presents a broken specimen after tensile testing, showing sections of the studied texture.

Figures 5–7 show the photos of fractures of the samples, BM, WM and HAZ respectively, after LCF tests. Conducted fractographic analysis revealed the differences in fracture mechanisms of the specimens cut out of BM (Figure 5) and of metal of the characteristic WJ zones after LCF tests.

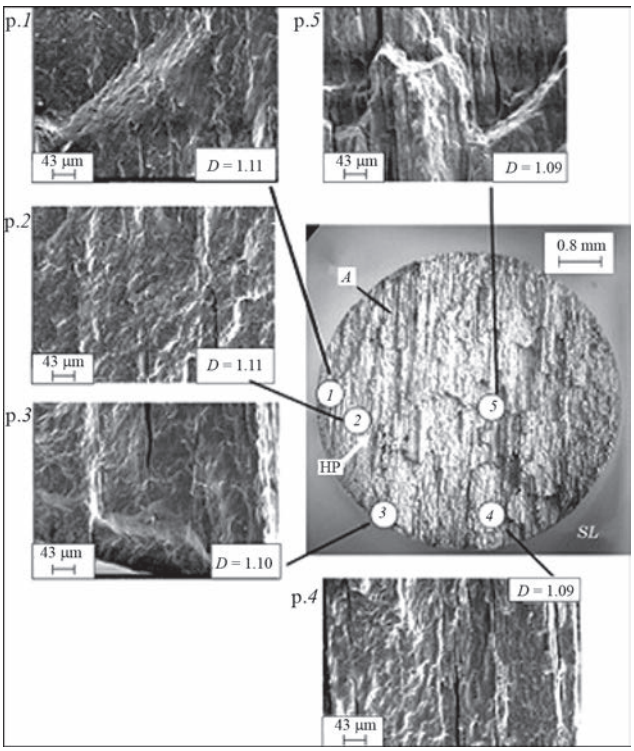

Figure 5. Fracture of BM specimen after LCF testing; *a*, *b* — view of a fragment of a broken specimen in (*L*–*T*) and (*L*–*S*) plane, respectively; *c* — fracture with typical macro- and microrelief (pp. *1*–*5*) of fracture; *HP* — fracture direction; *D* — fractal dimension

For specimens cut out of BM, quasibrittle fracture takes place with formation of secondary delamination cracks. This is promoted by BM {001} <110> crystallographic texture. Delamination can occur along the cleavage planes {001}.

Specimens, cut out of WM (Figure 6), fail by the pitting mechanism (ductile fracture). This is promoted by WM shear texture of {110} <001> type, which is the main one. It is reflected in decrease of FD value, compared to BM fracture (Figure 5).

Quasibrittle fracture is observed for HAZ specimens, but to a smaller extent, compared with BM, as a tensile-compressive crystallographic texture <001>–<110 > forms, which is due to slip deformation by {110} <110> and {110} <111> systems [17]. Here, grooved sections are observed on the HAZ microfractograms. FD value is close to its values for BM fracture specimen (Figure 5).

Figure 5 shows that the fractal dimension in different BM fracture sections changes from 1.09 to 1.11, average value of fractal dimension of base metal fracture surface was equal to $D_{av} = 1.10 \pm 0.01$. Similar results were demonstrated by analysis of fractal dimension of HAZ metal specimen. One can see from Figure 7, *c* that the fractal dimension in different HAZ fracture sections changes from 1.07 to 1.15, so that the average value of fractal dimension of fracture surface of the HAZ metal specimen was equal to $D_{av} = 1.11 \pm 0.01$.

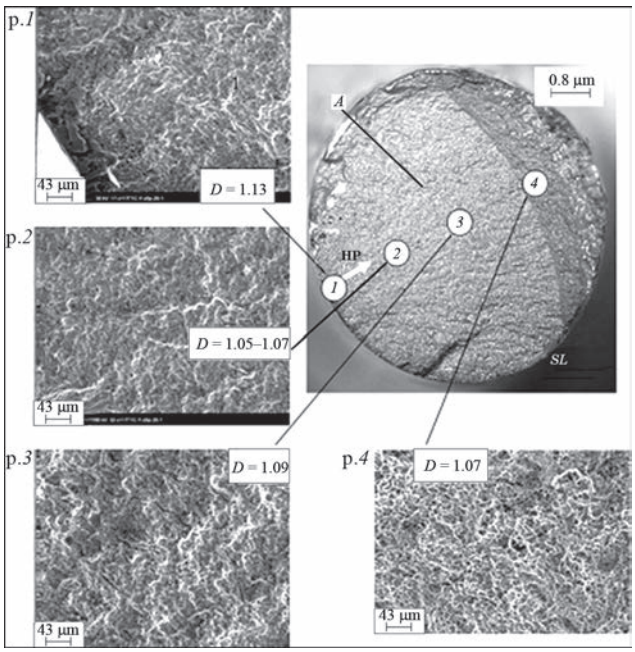

Figure 6. Fracture of a specimen from WM section after LCF testing: *a*, *b* — view of a fragment of the destroyed specimen in (*L*–*T*) and (*L*–*S*) plane, respectively; *c* — fracture with typical macro- (*A*) and microrelief (pp. *1*–*4*) of fracture; *HP* — fracture direction; *D* — fractal dimension

A more ductile fracture pattern of WM specimen follows from analysis of Figure 5 and texture. Here, fractal dimension in different sections of WM specimen fracture changed from 1.05 to 1.13 (Figure 6, *c*), and average value of WM fractal dimension was equal to $D_{av} = 1.08 \pm 0.01$.

It can be stated with 0.95 probability that the average value when taking a larger sample will not go beyond the above-mentioned ranges.

Thus, a tendency of fractal dimension increase during transition from the ductile (WM) to quasi-brittle facture pattern (BM and HAZ) is observed, that corresponds to lowering of the respective values of strength and ductility at static testing and shortening of the fatigue life. Increase of fractal dimension at quasibrittle fracture may mean that at quasiductile fracture the surface is "stretched" more due to presence of wider and deeper micropores. At the microscopic level the surface becomes smoother [18].

Increase of fractal dimension of the studied steel fractures at transition from the ductile to quasibrittle fracture agrees with the results of work [18] and other earlier studies. In [18] it is reported that the steel shows a decrease of fractal dimension at toughness increase. So, when studying [18] 24 series of specimens of AISI 4340 steel, it was shown that the fractal dimension of fracture of a steel specimen with 36 % fraction of the surface with ductile fracture was equal to $D \approx 1.28$. At increase of the ductile component fraction in the fracture to 50 % $D \approx 1.25$. At 77 % fraction of the ductile component in the fracture $D \approx 1.20$. At 100 % ductile fracture $D \approx 1.10$–1.09.

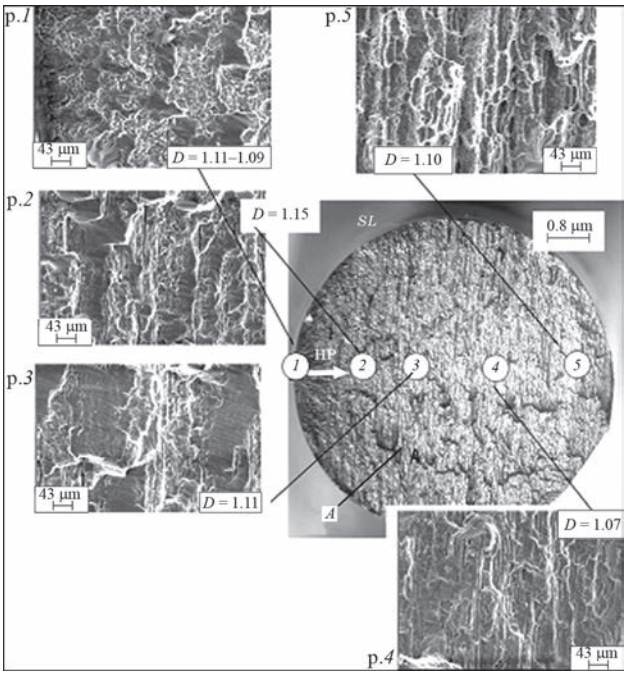

Figure 7. Fracture of a specimen from HAZ section after LCF testing: *a*, *b* — view of a fragment of broken specimen in (*L*–*T*) and (*L*–*S*) plane, respectively; *c* — fracture with typical macro- (*A*) and microrelief (pp. *1*–*5*) of fracture; *HP* — fracture direction; *D* — fractal dimension

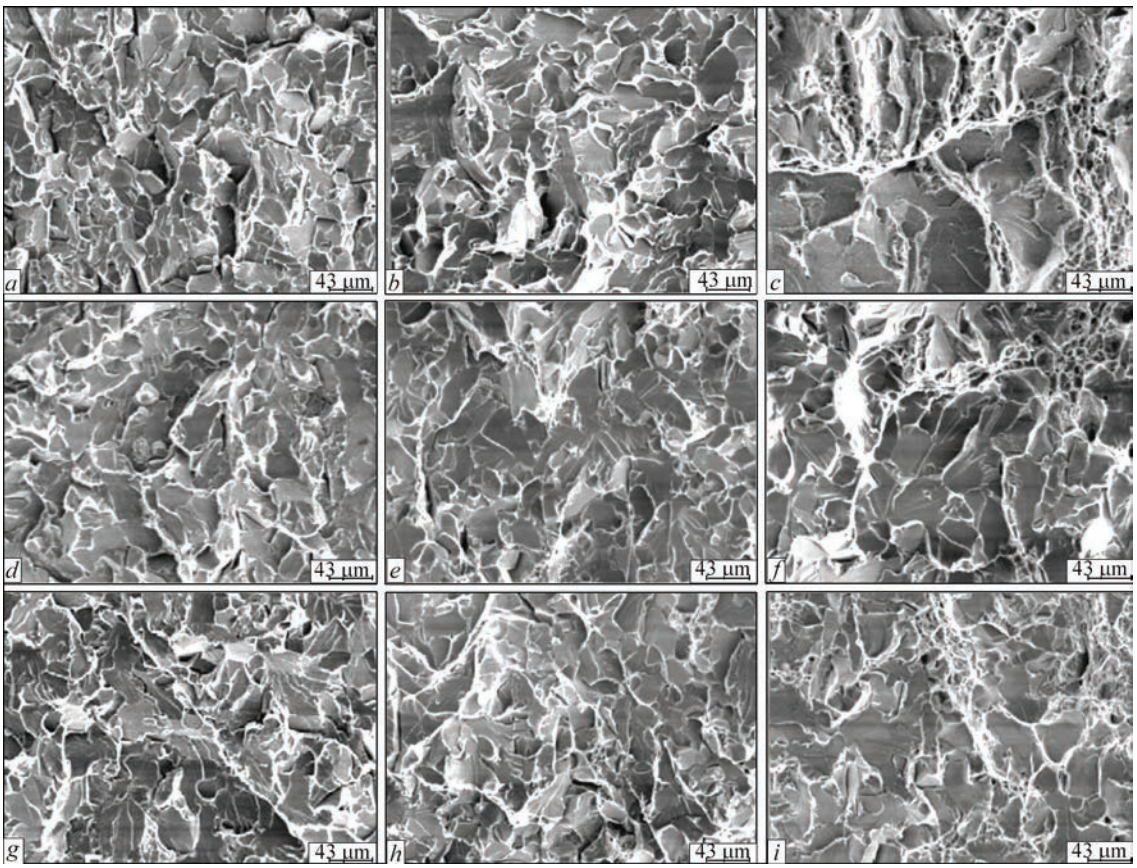

Figure 8. SEM photos of fractures after impact testing of specimens from 20 K grade steel. Scale bar length of 43 μm

Table 1. Chemical composition of metal of the studied cylinders, wt.%

Number	Service life, years	C	Mn	Si	S	P	Cr	Ni	C_{eq}
B1	45	0.513	1.01	0.319	0.023	0.023	0.14	0.11	0.72
B2	52	0.467	0.85	0.247	0.023	0.022	0.11	0.07	0.64
B3	18	0.490	0.88	0.255	0.019	0.026	0.23	0.10	0.69
B4	36	0.442	0.90	0.366	0.014	0.017	0.11	0.11	0.62
B5	49	0.482	0.72	0.257	0.026	0.019	0.10	0.08	0.63

Table 2. Fractal dimension (D_f) of fractures (Figure 8)

T, °C	LD	TD	DD	Average D_f
–50	1.59 ± 0.01	1.60 ± 0.01	1.64 ± 0.01	1.61 ± 0.01
20	1.55 ± 0.01	1.56 ± 0.01	1.59 ± 0.01	1.57 ± 0.01
50	1.52 ± 0.01	1.54 ± 0.01	1.55 ± 0.01	1.54 ± 0.01

Table 3. Fractal dimension (D_c) of P(t) diagrams (Figure 9)

T, °C	LD	TD	DD	Average D_f
–50	1.27 ± 0.01	1.23 ± 0.01	1.31 ± 0.01	1.27 ± 0.01
20	1.23 ± 0.01	1.17 ± 0.01	1.26 ± 0.01	1.22 ± 0.01
50	1.12 ± 0.01	1.13 ± 0.01	1.16 ± 0.01	1.14 ± 0.01

It should be noted that characterization of the fracture surfaces, using the above-mentioned average values of BM, HAZ and WM fractal dimensions is simplified. Presence of different values of fractal dimensions in different sections of corresponding fractures shows that the studied surfaces are multifractals, which can be interpreted as inseparable mixtures of simple fractals [17]. Each of them is characterized by its fractal dimension, and the entire respective fracture is described by an infinite set of fragments of destruction, associated with different probability of realization of different fragments in the set. Probability P_i of realization of each fragment is determined by the following relationship:

$$P_i = \ell_i^{\alpha}, \tag{9}$$

where α is the scaling parameter, $i = 1, 2, \ldots, N_n$ is the number of fragments in the set [17].

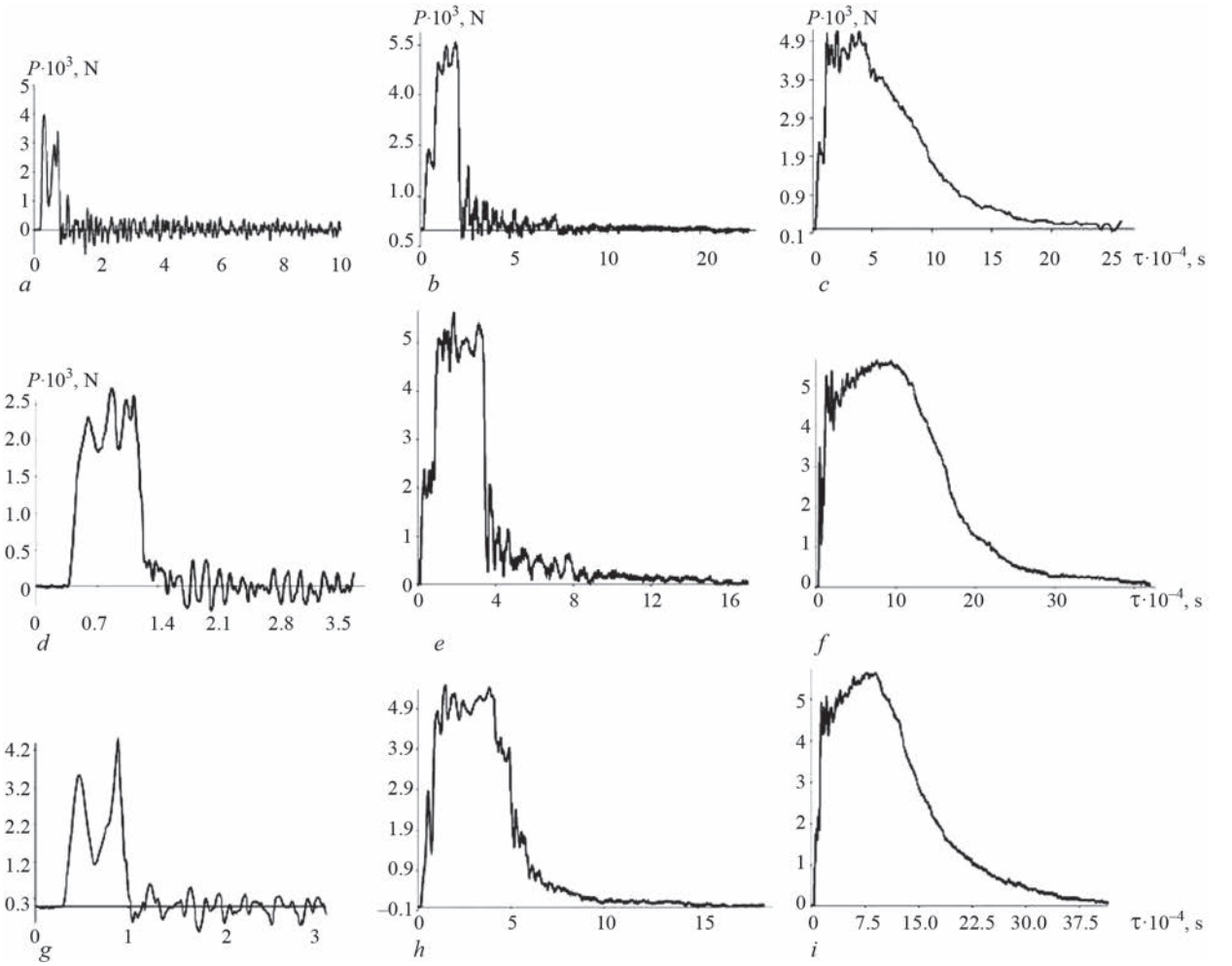

Figure 9. Diagrams of dependence of applied load P on time t at impact bend testing

Table 4. Specific fracture energy (J/m^2) at impact testing

Specimen number	–50 °C	20 °C	50 °C
Longitudinal direction LD			
1	0.83	5.04	22.87
2	0.73	4.31	20.82
Average value	0.78	4.67	21.84
Transverse direction TD			
1	0.97	9.88	47.95
2	0.95	10.91	57.95
Average value	0.96	10.39	52.95
Diagonal direction DD (LD + 45º)			
1	0.85	13.33	47.24
2	0.91	17.70	54.65
Average value	0.88	15.51	50.94

A detailed description of such fracture surfaces requires application of a multifractal approach [17, 19, 20] that may be the subject of future studies.

ANISOTROPY OF FRACTURE ENERGY AT IMPACT TESTING AND FRACTAL DIMENSION

Impact toughness parameters and fractal dimensions of load curves were determined, depending on testing time and respective fractures at impact bend testing of V-Charpy specimens, cut out in different directions from sheets of 20K steel in the temperature range from –50 to 50 °C [21]. Impact testing was conducted in a specialized vertical impact tester, fitted with a high-speed system for recording the deformations and forces [22]. Standard specimens with a V-shaped notch were cut out in three directions: longitudinal, transverse and at 45° angle to the longitudinal direction. Testing was conducted for three temperatures: –50 °C, 50 °C and room temperature, three specimens of each direction for each temperature. Test results were used to plot the diagrams of the change of the force in time $P(t)$ and the value of impact toughness was calculated by the procedure given in ISO 14556–2000 standard [23]. Figure 8 shows the microfractograms of fractures obtained in scanning electron microscope REM-200. The results of determination of fractal dimension D_f of the respective fractures are shown in Table 2. Figure 9 shows $P(t)$ diagrams of the change of the force with the time of impact bending testing of the specimens. The results of determination of fractal dimension D_c of the respective diagrams are shown in Table 3.

As one can see from Tables 2, 3 the behaviours of fractal dimensions D_f and D_c are similar. Both the FD values are maximal in the diagonal direction. Minimal values are observed at elevated testing temperature of +50 °C (Tables 2, 3).

At the same time, impact toughness at testing temperature of +50 °C is maximal (Table 4).

This is indicative of the ductile fracture pattern. Maximal values of fractal dimensions are in place at low testing temperature of –50 °C (Tables 2, 3). Impact toughness value is minimal at the same temperature (Table 1), which corresponds to brittle fracture pattern of the studied specimens at –50 °C.

Maximal values of fractal dimensions are observed for specimens, cut out in the diagonal direction (DD), i.e. FD anisotropy is in place (Tables 2, 3). This anisotropy can be caused by texture. It is found that the main component of the studied steel texture is {001} <110>. This is a typical component of rolling texture of BCC-steels [24]. In this case, crystallographic planes {001}, which are brittle cleavage planes in BCC-metals [27], are located normal to the diagonal direction. Cleavage can take place along these crystallographic planes that promotes a more brittle pattern of diagonal specimen fracture and is manifested in increase of the fractal dimension.

CONCLUSIONS

1. Configurations of brittle cracks in controlled rolled steel and AD1 aluminium are fractal, and brittle fracture shows a fractal pattern. Fractal model of the brittle crack was used to assess its critical dimensions R. For the studied steel, $R \approx 4.5$ μm, which corresponds to average size of cells of its dislocation structure. For AD1 aluminium critical size of brittle cracks is $R \approx 6.75$ μm.

2. At hydraulic testing of oxygen cylinders from Dc steel close correlation ties are in place between the fractal dimension of cylinder metal grains boundaries on the one hand, and impact toughness, bursting pressure at hydraulic testing and conditional yield limit with not lower than 0.80 correlation coefficients on the other hand. Low fractal dimension of grain boundaries corresponds to larger grain size, low values of impact toughness and yield limit, but high bursting pressure at hydraulic testing. Increase of fractal dimension of grain boundaries is accompanied by increase of im-

pact toughness, yield limit and lowering of bursting pressure. Respective correlation dependencies have the form of curves, reaching saturation with increase of fractal dimension of the boundaries. A transition from brittle transcrystalline cleavage to quasicleavage and ductile-brittle fracture pattern takes place with increase of fractal dimension.

3. Increase of the fraction of plastic deformation of the metal in the HAZ in the overall deformation amplitude at low-cycle fatigue testing of specimens of the characteristic zones of welded joint of a pipeline from 17G1S-U steel after its prolonged service leads to an essential lowering of cyclic fatigue life of the base and weld metal. There are significant differences in the fracture mechanisms: weld metal specimens fail by the pitting mechanism (ductile fracture), unlike quasibrittle fracture with formation of secondary delamination cracks, characteristic for base metal, and, to a smaller extent, for the heat-affected zone. This is accompanied by increase of average fractal dimension from 1.08 ± 0.01 for ductile fracture of the weld metal to 1.10 ± 0.01 for the base metal and to 1.11 ± 0.01 for the HAZ at quasibrittle fracture pattern. A connection can be traced between the fractal dimension of the fractures and fatigue life of the tested specimens. The fractal dimension value increases with fatigue life decrease.

4. Fractal dimensions of D_c diagram of $P(t)$ testing, which reflect the dependence of applied load P on time t, and fractal dimensions of fractures D_f after impact testing of specimens from 20K steel in the temperature range from –50 to 50 °C are of a similar nature. Maximum average values of both the fractal dimensions correspond to brittle fracture pattern and minimum impact toughness. Minimum average values of both the fractal dimensions correspond to ductile nature of fracture, and maximum impact toughness. The largest values of fractal dimension were found for specimens, cut out at 45° angle to the longitudinal direction, which are due to the influence of {001} <110> texture component, which is the main component of the low-alloyed texture of steel with BCC lattice. The presented results can be used for evaluation of the steel proneness to brittle fracture by analysis of fracture energy and fractal dimension of the diagrams of load dependence on time at impact toughness testing.

REFERENCES

1. Usov, V.V., Girenko, V.S., Rabkina, M.D. et al. (1993) Effect of the crystallographic texture on the anisotropy of fracture characteristics of control-rolled low-alloy steel. *Materials Sci.*, 29(**2**), 146–150. http://lib.gen.in/d55dae53541a8dc954b7f4d30d0a34cf.pdf
2. Lyakishev, N.P., Egiz, I.V., Shamraj, V.M. (2000) Texture and crystallographic peculiarities of fracture of steel X70 pipe material. *Metally*, **2**, 68–72 [in Russian]. http://www.imet.ac.ru/metally/nambers.htm
3. Ivanova, V.S., Balankin, A.S., Bunin, I.Zh., Oksagoev, A.A. (1994) *Synergy and fractals in materials science.* Moscow, Nauka [in Russian]. https://www.researchgate.net/publication/268999858_Sinergetika_i_fraktaly_v_materialovedenii
4. Mandelbrot, B. (2002) *Fractal geometry of nature.* Moscow, Institute for Computer Research. https://ruwapa.net/book/benua-mandelbrot-fraktalnaya-geometriya-prirody/
5. Watanabe, T., Tsurekawa, S. (2004) Toughening of brittle materials by grain boundary engineering. *Mater. Sci. Engng. A.*, **387–389**, 447–455. https://www.researchgate.net/publication/222146139_Toughening_of_Brittle_Materials_by_Grain_Boundary_Engineering
6. Vitek, V., Chen, S.P., Voter, A.F. et al. (1989) Grain boundary structure and intergranular fracture in L12 ordered alloys. *Mater. Sci. Forum,* **46**, 237–252. https://www.scientific.net/MSF.46.23
7. Watanabe, T. (1993) Grain boundary design and control for high temperature materials. *Mater. Sci. Engng. A.*, **166**, 11–28. https://www.sciencedirect.com/science/article/abs/pii/092150939390306Y
8. Zhou, H.W., Xie, H. (2003) Direct estimation of the fractal dimensions of a fracture surface of rock. *Surface Review and Letters*, 10(**5**), 751–762. https://paperzz.com/doc/9119828/direct-estimation-of-the-fractal-dimensions-of-a
9. Lucas, M.A. (2012) *Foundations of measurement fractal theory for the fracture mechanics applied. in fracture mechanics*. Edited by Alexander Belov. https://www.intechopen.com/chapters/41469
10. *Harfa: download*. http://www.fch.vut.cz/lectures/imagesci/includes/harfa_download.inc.php
11. *ACDSee Professional 2019*. https://www.acdsee.com/en/products/photo-studio-professional
12. Usov, V.V., Shkatulyak, N.M. (2005) Fractal nature of the brittle fracture surfaces of metal. *Materials Sci.*, 41(**1**), 62–66. https://www.researchgate.net/publication/226818869_Fractal_Nature_of_the_Brittle_Fracture_Surfaces_of_Metal
13. Mosolov, A.B. (1991) Fractal Griffith crack. *Zhurn. Tekh. Fiz.*, 64(**7**), 57–60 [in Russian]. http://journals.ioffe.ru/articles/viewPDF/24666
14. Honeycomb, R. (1962) *Plastic deformation of metals*. Moscow, IL [in Russian]. https://ua1lib.org/book/2433166/2721d7
15. Bernshtejn, M.L., Zajmovsky, M.A. (1979) *Mechanical properties of metals*. Moscow, Metallurgiya [in Russian]. https://ua1lib.org/book/2720875/410310
16. Usov, V.V., Rabkina, M.D., Shkatulyak, N.M., Cherneva, T.S. (2015) Fractal dimension of grain boundaries and mechanical properties of the metal of oxygen cylinder. *Material Sci.*, 50(**4**), 612–620. https://www.researchgate.net/publication/276456141_Fractal_Dimension_of_Grain_Boundaries_and_Mechanical_Properties_of_the_Metal_of_Oxygen_Cylinders
17. Usov, V.V., Gopkalo, E.E., Shkatulyak, N.M. et al. (2015) Texture, microstructure, and fractal features of the low cycle fatigue failure of the metal in pipeline welded joints. *Russian Metallurgy (Metally)*, **9**, 759–770. https://www.researchgate.net/publication/289569432_Texture_microstructure_and_fractal_features_of_the_low-cycle_fatigue_failure_of_the_metal_in_pipeline_welded_joints
18. Carney, L.R., Mecholsky, J.J. (2013) Relationship between fracture toughness and fracture surface fractal dimension in AISI 4340 steel. *Mater. Sci. Applicat*., 4(**4**), 258–267. DOI: http://dx.doi.org/10.4236/msa.2013.44032
19. Glushkov, A., Khetselius, O., Brusentseva, S., Duborez, A. (2014) Modeling chaotic dynamics of complex systems with

using chaos theory, geometric attractors, quantum neural networks. *Proc. Int. Geom. Center*, 7(**3**), 87–94, http://eprints.library.odeku.edu.ua/id/eprint/2938/1/%D0%93%D0%BB%D1%83%D0%A5%D0%B5%D1%86%D0%91%D1%80%D1%83%D0%94%D1%83%D0%B1Pmgc_2014_7_3_13%20(1).pdf
20. Glushkov, A.V., Buyadzhi, V.V., Ternovsky, V.B. et al. (2018) A chaos-dynamical approach to analysis, processing and forecasting measurements data of the chaotic quantum and laser systems and sensors. *Sensor Electronics and Microsystem Technologies*, 15(**4**) 41–49, http://eprints.library.odeku.edu.ua/id/eprint/4481/1/2018%20T15%20%234%20CEMST.pdf
21. Usov, V., Rabkina, M., Shkatulyak, N. et al. (2020) Anisotropy of Fractal Dimensions of Fractures and Loading Curves of Steel Samples During Impact Bending. *Material Sci.* 17(**4**), 142–151. http://ijmse.iust.ac.ir/article-1-1680-en.pdf
22. Kondryakov, E.A., Zhmaka, V.N., Kharchenko, V.V. et al. (2005) System of Strain and Load Measurement in Dynamic Testing of Materials. *Strength Mater.*, **37**, 331–335. https://doi.org/10.1007/s11223-005-0046-6
23. *Steel. Charpy impact V-notch test. Instrumental test method* [in Russian]. http://rossert.narod.ru/alldoc/info/2z77/g39315.html
24. (2015) *Oil and Gas Pipelines: Integrity and Safety*: Handbook. Winston R. by Ed. https://www.worldcat.org/title/oil-and-gas-pipelines-integrity-and-safety-handbook/oclc/904715784
25. Pineau, A., Benzerga, A.A., Pardoen, T. (2016) Failure of metals I: Brittle and ductile fracture. *Acta Materialia*, **107**, 424–483. https://par.nsf.gov/servlets/purl/10019128Pineau

ORCID
V.V. Usov: 0000-0001-7855-5370,
M.D. Rabkina: 0000-0003-3498-0716,
N.M. Shkatulyak: 000-0003-4905-001X,
N.I. Rybak: 0000-0003-2061-0642,
O.O. Stofel: 0000-0002-0315-5484

CONFLICT OF INTEREST
The Authors declare no conflict of interest

CORRESPONDING AUTHOR
V.V. Usov
E.O. Paton Electric Welding Institute of the NASU
11 Kazymyr Malevych Str., 03150, Kyiv, Ukraine
E-mail: valentinusov67@gmail.com

SUGGESTED CITATION
V.V. Usov, M.D. Rabkina, N.M. Shkatulyak, N.I. Rybak, O.O. Stofel (2022) Application of fractal analysis in diagnostics of technical condition of metal structure elements. *The Paton Welding J.*, **4**, 51–60.

JOURNAL HOME PAGE
https://pwj.com.ua/en

Received: 16.12.2021
Accepted: 30.06.2022

SUBSCRIPTION–2022

«The Paton Welding Journal» is Published Monthly Since 2000 in English, ISSN 0957-798X, doi.org/10.37434/tpwj.

«The Paton Welding Journal» can be also subscribed worldwide from catalogues subscription agency EBSCO.

If You are interested in making subscription directly via Editorial Board, fill, please, the coupon and send application by Fax or E-mail.

12 issues per year, back issues available.

$384, subscriptions for the printed (hard copy) version, air postage and packaging included.

$312, subscriptions for the electronic version (sending issues of Journal in pdf format or providing access to IP addresses).

Institutions with current subscriptions on printed version can purchase online access to the electronic versions of any back issues that they have not subscribed to. Issues of the Journal (more than two years old) are available at a substantially reduced price.

SUBSCRIPTION COUPON

Address for journal delivery _____

_____

Term of subscription since _____ **20** **till** _____ **20** _____

Name, initials _____

Affiliation _____

Position _____

Tel., Fax, E-mail _____

The archives for 2009–2020 are free of charge on www://patonpublishinghouse.com/eng/journals/tpwj

ADVERTISING

in «The Paton Welding Journal»

External cover, fully-colored:
First page of cover (200×200 mm) — $700
Second page of cover (200×290 mm) — $550
Third page of cover (200×290 mm) — $500
Fourth page of cover (200×290 mm) — $600

Internal cover, fully-colored:
First/second/third/fourth page (200×290 mm) — $400

Internal insert:
(200×290 mm) — $340
(400×290 mm) — $500

- Article in the form of advertising is 50 % of the cost of advertising area
- When the sum of advertising contracts exceeds $1001, a flexible system of discounts is envisaged
- Size of Journal after cutting is 200×290 mm

Address
11 Kazymyr Malevych Str. (former Bozhenko Str.), 03150, Kyiv, Ukraine
Tel.: (38044) 205 23 90
Fax: (38044) 205 23 90
E-mail: journal@paton.kiev.ua
www://patonpublishinghouse.com/eng/journals/tpwj